Non-destructive detection of matrix stabilization correlates with enhanced mechanical properties of self-assembled articular cartilage

A.K. Haudenschild[a], **B.E. Sherlock**[a], **X. Zhou**[a], **J.C. Hu**[b], **J.K. Leach**[a,c], **L. Marcu**[a], and **K.A. Athanasiou**[b]

[a]Department of Biomedical Engineering, University of California Davis, Davis, CA, USA

[b]Department of Biomedical Engineering, University of California Irvine, Irvine, CA, USA

[c]Department of Orthopaedic Surgery, University of California Davis Medical Center, Sacramento, CA, USA

Abstract

Tissue engineers rely on expensive, time-consuming, and destructive techniques to monitor the composition, microstructure, and function of engineered tissue equivalents. A non-destructive solution to monitor tissue quality and maturation would greatly reduce costs and accelerate the development of tissue engineered products. The objectives of this study were to 1) determine whether matrix stabilization with exogenous lysyl oxidase like protein-2 (LOXL2) with recombinant hyaluronan and proteoglycan link protein-1 (LINK) would result in increased compressive and tensile properties in self-assembled articular cartilage constructs, 2) evaluate whether label-free, non-destructive, <u>F</u>luorescence <u>L</u>ifetime <u>Im</u>aging (FLIm) could be used to infer changes in both biochemical composition and biomechanical properties, 3) form quantitative relationships between destructive and nondestructive measurements to determine whether the strength of these correlations are sufficient to replace destructive testing methods, and 4) determine whether support vector machine (SVM) learning can predict LOXL2-induced collagen crosslinking. The combination of exogenous LOXL2 and LINK proteins created a synergistic 4.9-fold increase in collagen crosslinking density and an 8.3-fold increase in tensile strength as compared to control (CTL). Compressive relaxation modulus was increased 5.9-fold with addition of LOXL2 and 3.4-fold with combined treatments over CTL. FLIm parameters had strong and significant correlations with tensile properties (R^2=0.82; p<0.001) and compressive properties (R^2=0.59; p<0.001). SVM learning based on FLIm-derived parameters was capable of automating tissue maturation assessment with a discriminant ability of 98.4%. These results showed marked improvements in mechanical properties with matrix stabilization and suggest that FLIm-based tools have great potential for the non-destructive assessment of tissue engineered cartilage.
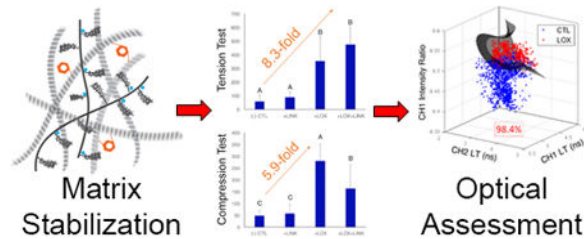
Correspondence and reprint requests should be addressed to: Kyriacos A. Athanasiou, Ph.D., Department of Biomedical Engineering, University of California Irvine, 3120 Natural Sciences II, Irvine, CA 92697-2715, USA, Fax: (949) 824-1727, Telephone: (949) 824-9196, athens@uci.edu.

Athanasiou and Marcu should be considered joint senior authors.

Graphical Abstract

1 Introduction

The tissue engineering and regenerative medicine industries have an immense potential to improve the clinical outcome and deliver effective curative therapies to a number of chronic diseases that are currently beyond repair. The U.S. Food and Drug Administration (FDA) has outlined a series of guidance documents for the clinical application of tissue engineered products that specify thorough characterization during the development and manufacturing process and defined acceptance criteria for product release (FDA, 2011). In current practice, tissue engineers rely on a battery of expensive, time-consuming, and destructive techniques to monitor the composition, microstructure, and function of engineered tissue equivalents. A non-destructive solution to monitor tissue quality and maturation would address the significant hurdles that these new regulations pose for the translation of cell-based tissue products into the clinic, greatly reduce costs, speed the development of tissue products, and allow clinical evaluation of current and emerging therapeutic interventions.

Quantitative optical techniques based on endogenous tissue autofluorescence have been developed to image and non-destructively characterize tissue properties (Gorpas, *et al.*, 2015, Gorpas, *et al.*, 2016, Sun, *et al.*, 2012). A number of endogenous biomolecules, including the extracellular matrix (ECM) protein collagen (Alfonso-Garcia, *et al.*, 2018) and its crosslinks (Wagnieres, *et al.*, 1998), and proteoglycans (Angheloiu, *et al.*, 2011) give rise to tissue autofluorescence. The relative concentration and distribution of individual fluorophores within the tissue create unique fluorescence emission profiles that can be quantified. Fluorescence Lifetime Imaging (FLIm) utilizes the exponential decay rate of these endogenous fluorophores, termed the fluorescence lifetime (LT), to generate images of tissue biochemistry and can be implemented in a single, narrow and flexible fiber-optic interface between the apparatus and the sample (Marcu, *et al.*, 2014). Fiber-based FLIm has been used to detect native cartilage matrix depletion and correlated with changes in mechanical properties (Haudenschild, *et al.*, 2018). Data processing techniques have been developed to allow near real-time acquisition (Marcu, *et al.*, 2014) and quantification (Liu, *et al.*, 2012) of FLIm parameters to detect biochemical changes in various biological tissues, both *in vitro* and *in vivo* (Fite, *et al.*, 2011, Manning, *et al.*, 2013, Yankelevich, *et al.*, 2014).

In addition to monitoring the changes in biochemical composition during tissue development and maturation, it is also necessary to quantify changes in the mechanical properties of both native and engineered replacement tissues to determine successful tissue functionality. Articular cartilage is a load-bearing tissue comprised of primarily collagen type II, proteoglycans, and water (Zhang, *et al.*, 2009), where there is a direct structure-function relationship between the mechanical properties and the biochemical composition of the tissue (Setton, *et al.*, 1993) (Figure 1A). Articular cartilage compressive properties are strongly associated with proteoglycan content. Hyaluronan and proteoglycan link protein-1 (LINK) is a glycoprotein that stabilizes the interaction between the major proteoglycan structural components, aggrecan and hyaluronic acid (Hardingham, 1979, Seyfried, *et al.*, 2005) creating large, negatively-charged aggregates. The resulting LINK-stabilized aggregates imbibe water and provide cartilage with its osmotic properties, which are critical to its ability to resist compressive loads (Kiani, *et al.*, 2002, Wang, *et al.*, 2013). Articular cartilage tensile properties are strongly associated with collagen and collagen crosslinking content. Despite recent advances, tissue engineered cartilage currently lacks the mechanical strength of native tissue (Huey, *et al.*, 2012a). The addition of exogenous LINK protein to both aggrecan solutions (Tang, *et al.*, 1996), isolated cells (Plaas, *et al.*, 1988), and cell seeded hydrogel constructs (Han, *et al.*, 2010) has shown that aggrecan retention through LINK-mediated stabilization is associated with increased compressive modulus. Similarly, the addition of the exogenous collagen crosslinking enzyme lysyl oxidase-like 2 protein (LOXL2) produces stable pyridinoline (PYR) crosslinks and enhances tensile strength (Makris, *et al.*, 2013). The success of tissue engineered articular cartilage replacement products *in vivo* depends heavily on the development of sufficient tensile and compressive properties (Huey, *et al.*, 2012b, Makris, *et al.*, 2015, Responte, *et al.*, 2007). The development of quantitative, validated tools optimized specifically for monitoring the biochemical and mechanical properties of tissue engineered articular cartilage are essential for evaluating these and other methods of improving tissue functionality (Morgan, *et al.*, 2014).

The ideal system for monitoring tissue maturation and development would allow repeated sterile measurements of developing tissue and incorporate some degree of automation to both sample assessment and data processing to determine whether release criteria are met prior to clinical use. A Support Vector Machine (SVM) is a supervised machine learning technique that is widely used for classification of data into separate groups. The SVM algorithm uses a series of past observations or training data to learn how to automatically make accurate classification predictions about new, unknown data. The SVM divides separate experimental groups by constructing a multidimensional hyperplane decision boundary that maximizes the gap between the two group's data clusters. The SVM algorithm achieves high discriminative power between the groups by using nonlinear functions called kernels to transform the input space into a multidimensional space (Yu, *et al.*, 2010). Previous studies have shown that SVM analysis can predict the proteoglycan content of tissue engineered cartilage (Irrechukwu, *et al.*, 2012, Lin, *et al.*, 2012). Further efforts are needed to determine the predictive capabilities of SVM algorithms in identifying collagen crosslinking content in tissue engineered articular cartilage.

The overall goal of this work is to study whether nondestructive optical methods have the potential to replace the conventional destructive measurements of tissue engineered articular cartilage properties in an effort to reduce costs and research time, and to allow for time-lapse measurements that track the maturation of individual samples. The objectives of this study were to 1) determine whether matrix stabilization though the addition of exogenous LOXL2 and LINK proteins would result in increased compressive and tensile properties in self-assembled articular cartilage constructs, 2) evaluate whether label-free, non-destructive, FLIm could be used to infer the changes in both biochemical composition and biomechanical properties of tissue-engineered cartilage, 3) form specific, quantitative relationships between destructive and nondestructive measurements to determine whether the strength of these correlations are sufficient to replace destructive testing methods, and 4) determine whether SVM learning can predict LOXL2-induced collagen crosslinking in tissue engineered articular cartilage. We hypothesized that FLIm could infer increases in both biochemical composition and biomechanical properties of self-assembled articular cartilage created through matrix stabilization with LOXL2 and LINK proteins and that a SVM built on FLIm-based parameters could identify collagen crosslinking.

2. Materials and Methods

2.1 Chondrocyte isolation

Articular cartilage was harvested from the femoral condyles of five juvenile bovine stifle joints (Research 87, Boston, MA), minced, and digested in Dulbecco's Modified Eagle Medium (DMEM) with high glucose/GlutaMAX™-I (Life Technologies, Grand Island, NY) with 5% fetal bovine serum (FBS) (HyClone, GE Healthcare Life Sciences, Marlborough, MA), 0.3% collagenase type II (Worthington, Lakewood, NJ), and 1% penicillin/streptomycin/fungizone (P/S/F) (Lonza, Basel, Switzerland) for 18h on an orbital shaker at 37 °C. Following digestion, the cells were filtered through 70 μm cell strainers, and washed 3 times with DMEM. All donor cells were pooled prior to construct formation.

2.2 Self-assembled construct culture

Constructs were formed using the self-assembling process, as previously described (Hu and Athanasiou, 2006). Briefly, 4×10^6 chondrocytes were suspended in 100 μL of a chondrogenic control medium (Kwon, *et al.*, 2017) consisting of DMEM with 1% ITS+ premix (BD Biosciences, Bedford, MA), 1% non-essential amino acids (NEAA) (Life Technologies), 50 μg/mL ascorbate-2-phosphate (Sigma-Aldrich, St. Louis, MO), 40 μg/mL L-proline (Sigma-Aldrich), 100 μg/mL sodium pyruvate (Sigma-Aldrich), and 100 nM dexamethasone (Sigma-Aldrich), and 1% P/S/F. Cell suspensions were seeded in non-adherent wells (5 mm diameter, 2% agarose) in 24-well plates (Costar, Corning, NY). After 4h, 400 μL of control medium were added to each well. Self-assembled constructs were cultured for 4 weeks in control medium only (CTL), CTL with 0.2 μg/mL of recombinant human LINK (R&D systems, Minneapolis, MN) added for weeks 0–2 (+LINK), CTL with 0.146 μg/mL hydroxylysine (Sigma-Aldrich), 0.0016 mg/mL copper sulfate (Sigma-Aldrich), and 0.15 μg/mL of LOXL2 (SignalChem, Richmond, British Columbia, Canada) added for weeks 1–3 (+LOX), or a combination of both exogenous factors (+LOX+LINK)

(Figure 1B). Constructs were removed from wells at day 5 and 1 mL of fresh media was exchanged daily.

2.3   Non-destructive optical assessment of self-assembled articular cartilage

At week 4 in culture, a fiber-based, label-free fluorescence-based imaging system was used to make a non-destructive assessment of each cartilage construct (n=6 per condition), followed by dissection for biochemical assays, mechanical evaluation, and histological processing (Figure 2A). The underlying principle of operation of the FLIm system has been previously reported (Sun, *et al.*, 2009, Yankelevich, *et al.*, 2014). Time-resolved fluorescence was acquired by both systems using the pulse sampling technique (Marcu, *et al.*, 2014), and the decays were parameterized in post-processing using a constrained least-squares deconvolution with Laguerre expansion (Liu, *et al.*, 2012). Average fluorescence lifetimes (LT) were calculated using the definition of intensity-weighted average lifetime (Yankelevich, *et al.*, 2014). A microchip laser (STV-02E-1×0, TEEM photonics, Grenoble, France) emitted optical pulses at a wavelength of 355 nm to generate sample autofluorescence. Light was delivered to and collected from the sample using a 2m long, flexible fiber optic cable (Molex, Lisle, IL) with an outer diameter of 480 μm. For optical assessment, the central 5 mm diameter cylindrical core (0.7 – 1.7 mm thick; Supplemental Figure S3) from each sample was placed in a custom, glass sample holder in a PBS bath at room temperature. During imaging, the distal tip of the fiber was positioned approximately 1 mm above and perpendicular to the neocartilage surface. A two-axis digital translation stage (MX80L, Parker, Cleveland, OH) was used to scan the fiber across the sample surface. Complete mapping of the surface of each sample occurred in under 10 minutes and samples were returned to 37°C immediately following imaging. The attenuation of 355 nm light in cartilage limits the penetration depth of FLIm to ~300 μm below the sample surface (Descalle, *et al.*, 1998).

For FLIm, the fluorescence emission was separated into four spectral bands (CH1 = 375–410 nm, CH2 = 450–485 nm, CH3 = 515–565 nm, CH4 = 595–660 nm) using a custom-built wavelength selection module. Each spectral band had an associated fiber optic delay line of different lengths (longer wavelength bands have longer delay lines). This arrangement allowed the four spectral bands to be temporally multiplexed onto a single photomultiplier tube (PMT) (R5916U-50, Hamamatsu, Bridgewater, NJ), the voltage from which was digitized using a high speed data acquisition board (DAQ) (PXIe-5185, National Instruments, Austin, TX) operating with a temporal resolution of 80 ps. This enabled complete mapping of the surface of the sample in approximately 10 minutes at a resolution of 200 μm/pixel. The mean and standard deviation of fluorescence lifetime in each spectral band were extracted from the FLIm images (Figure 2B) by defining circular regions of interest, centered on the sample that encompassed >75% of the surface area.

2.4   Biochemical analysis and histology

For biochemical analysis, tissue samples were measured to obtain wet (ww) and dry (dw) weights. Lyophilized samples were digested in papain for 18h at 60°C, as previously described (Kochiadakis, *et al.*, 2001). Sulfated GAG content was assayed using the Blyscan Glycosaminoglycan Assay kit (Biocolor, Westbury, NY). Total collagen content was

quantified using a hydroxyproline assay (Biocolor) (Woessner, 1961). Pyridinoline (PYR) collagen crosslinks were analyzed and quantified by high-performance liquid chromatography (HPLC), as previously described (Bank, *et al.*, 1997). Constructs were acid digested and suspended in a solution of 0.5% heptafluorobutyric acid (HFBA) in 10% acetonitrile. Samples were injected into a Luna C18 column (Phenomenex, Torrance, CA) and eluted on a HPLC system (Prominence UFLC, Shimadzu, Columbia, MD). A linear calibration curve was created using PYR standards (Quidel, San Diego, CA) for crosslink quantification. Collagen crosslinking density was defined as the molar ratio of PYR per collagen molecule and calculated assuming the molecular weight of the collagen triple helix of 300,000 MW (Haus, *et al.*, 2007).

For histological evaluation, samples were fixed in 10% neutral buffered formalin, paraffin embedded, and then sectioned at 10 μm. Sections were stained with hematoxylin and eosin (H&E) for general morphology, safranin O and nuclear fast green for glycosaminoglycans, or picrosirius red and nuclear fast green for total collagen following routine procedures. Picrosirius red stained collagen was visualized under polarized light microscopy to enhance natural birefringence (Junqueira, *et al.*, 1979, Puchtler, *et al.*, 1973).

2.5 Compressive and tensile testing

Compressive properties were quantified by coring a 2 mm cylindrical punch from each construct, as previously described (Allen and Athanasiou, 2006). Briefly, compression testing is accomplished in two phases: height detection and stress relaxation testing in unconfined compression. Samples were equilibrated in a PBS bath, loaded to 0.02N load to determine sample thickness, and preconditioned under 15 cycles of 5% strain. Samples were loaded under 10% strain for 600 s immediately followed by 20% strain for 900 s to obtain equilibrium (Figure S1). Force-displacement data were recorded, converted to stress-strain based on sample dimensions, and all data were analyzed using biphasic theory (Mak, *et al.*, 1987) in Matlab (Mathworks, Natick, MA) to calculate instantaneous modulus, relaxation modulus, and coefficient of viscosity for each sample.

Tensile testing was conducted using a uniaxial materials testing machine (Test Resources, Shakopee, MN), as previously described (Makris, *et al.*, 2013). Briefly, cartilage samples were cut into dog-bone shaped tensile specimens and the sample thickness and width were measured via ImageJ software (NIH, Bethesda, MD) (Schindelin, *et al.*, 2015). A uniaxial strain to failure test was conducted with a fixed gauge length of 1.3 mm and a strain rate of 1% of the gauge length per s. Load-displacement curves were normalized to specimen cross-sectional area and the apparent Young's Modulus was calculated by least squares fitting the linear portion of the resulting stress-strain curve in Matlab (Mathworks). Ultimate tensile strength (UTS) was defined at the maximum stress.

2.6 Statistical analysis and modeling

All evaluations in this study were performed using n=6 matched samples per treatment group on JMP v13 (SAS Institute, Cary, NC). Statistical analysis of groups was performed using one-way ANOVA with Tukey's *post-hoc* analysis. Bar chart data are presented as mean ± standard deviation with significant differences ($p < 0.05$) indicated by bars not

sharing the same letter. Bars with the same letter are not significantly different from one another and bars with more than one letter reflect overlap between groups. Correlations between bivariate parameters of each treatment were modeled separately to determine which outcome parameter correlated with which biochemical component using simple linear least squares regression analysis.

2.7   Support vector machine development

Support Vector Machine (SVM) algorithms with a (Gaussian) Radial Basis Function (RBF) kernel (Chang and Lin, 2011, Wang, *et al.*, 2011) were tested for their ability to predict LOXL2-induced collagen crosslinking in self-assembled constructs. The feature vector included average fluorescence lifetime and intensity values from CH1, CH2, and CH3. Due to the range of FLIm signal across the engineered tissue samples, we defined the accuracy of the classification as the ratio of correctly classified pixels to the total number of pixels in the image. Artifacts due to low signal to noise ratio and edge effects were removed by data thresholding. A receiver operating characteristic curve was generated to evaluate the quality of a binary classification test and to graphically illustrate the diagnostic ability of the SVM classifier as the discriminant threshold was varied. Sensitivity, specificity, and positive predictive values were calculated using a leave-one-out cross-validation approach (Hsu and Lin, 2002). This involved sequentially leaving data from a single specimen out of the training set, then testing the classification accuracy on that single specimen for all specimens. Data processing, image analysis, and classification were performed using MATLAB (Mathworks).

3.   Results

3.1   Exogenous LOXL2 and LINK proteins enhanced extracellular matrix stabilization in self-assembled constructs

The self-assembling process resulted in flat, uniform neocartilage formation in all culture conditions tested (Figure 3A). Matrix stabilization with LOXL2 and LINK proteins resulted in increased collagen birefringence and proteoglycan (Gago, *et al.*) staining as compared to CTL (Figure 3B). Proteoglycan content was significantly increased with both +LOX and +LOX+LINK treatments (1.5- and 1.4-fold respectively, p<0.001) (Figure 4A). Treatment did not significantly alter collagen content (p=0.43; 4.64 ± 0.57% COL/dw for all groups), but both +LOX and +LOX+LINK treatments produced large increases in collagen crosslinking density (2.9- and 4.9-fold respectively, p<0.0001) (Figure 4B).

3.2   Matrix stabilization improved both tensile and compressive mechanical properties

The relaxation modulus was significantly increased with both +LOX and +LOX+LINK treatments as compared to CTL (5.9- and 3.4-fold respectively, p<0.001) (Figure 4C). Similarly, the instantaneous modulus was significantly increased with both +LOX and +LOX+LINK treatments as compared to CTL (3.9- and 2.1-fold respectively, p<0.001) (Figure 4D). The coefficient of viscosity was significantly increased with +LOX treatment as compared to CTL (7.2-fold, p<0.0001) (Figure S2B). Compared to CTL, tensile Young's Modulus significantly increased 2.0-fold with +LOX and 3.8-fold with +LOX+LINK treatment to reach an average value of 1.98 ± 0.68 MPa (p<0.01) (Figure 4E). UTS was also

significantly increased with both +LOX and +LOX+LINK treatments as compared to CTL (6.2- and 8.3-fold respectively, p=0.001) (Figure 4F).

3.3 Destructive and non-destructive testing detect changes in matrix stabilization and mechanical properties

FLIm CH1 and CH3 LT were significantly increased with the addition of exogenous proteins (p<0.001 and p=0.02, respectively) (Figure 4G and4H). Destructive biochemical assays had strong significant correlations with both tensile and compressive mechanical properties. Proteoglycan content (GAG/ww) had a strong and significant correlation with compressive modulus (R^2=0.68; p<0.001) (Figure 5A). Ultimate tensile strength had a strong and significant correlation with collagen crosslinking density (PYR/COL) (R^2=0.63; p<0.001) (Figure 5B). Non-destructive fluorescence LT was able to detect changes in biochemical content. FLIm CH3 LT had moderate significant correlation with GAG/ww (R^2=0.49; p=0.001) (Figure 5C) and FLIm CH1 LT has a significant correlation with PYR/COL (R^2=0.45; p=0.002) (Figure 5D). Non-destructive fluorescence LT was able to detect changes in both tensile and compressive mechanical properties. FLIm CH3 LT had a strong and significant correlation with compressive modulus (R^2=0.59; p<0.001) (Figure 5E). FLIm CH1 LT had a strong and significant correlation with the ultimate tensile strength (R^2=0.82; p<0.0001) (Figure 5F) and a moderate significant correlation with the coefficient of viscosity (R^2=0.50; p<0.002) (Figure S2B).

3.3 Support vector machine (SVM) learning identifies LOXL2-induced collagen crosslinking in tissue engineered neocartilage

SVM classification was able to identify LOXL2-induced collagen crosslinking in the self-assembled neocartilage using fluorescence-based parameters. Fluorescence LT in all 3 spectral channels increased with +LOX treatment as compared to control and allowed +LOX detection as observed from parameter distributions (Figure 6A). A SVM was built using the three fluorescence-based parameters CH1 intensity ratio, CH1 LT, and CH2 LT. The three-dimensional scatter plot of training data shows the SVM classifier hyperplane as a decision boundary for +LOX classification (Figure 6B). The area under the curve was used to determine the discriminant ability of the SVM classifier as 98.4% (Figure 6C). The diagnostic ability of the SVM was dependent on the number of pixels analyzed in the region of interest with higher pixel numbers improving the discriminant ability of the classification. Increasing pixel number from 100 to 500 pixels improved sensitivity (true positive rate) from 0.94 to 0.98 and improved specificity (1-false positive rate) from 0.75 to 0.88 (Figure 6D).

4. Discussion

The novel findings of this study include 1) enhanced tensile and compressive properties (8.3- and 5.9-fold , respectively) through matrix stabilization with a combination of LOXL2 and LINK proteins, 2) quantitative relationships between FLIm CH3 LT signal and compressive relaxation modulus (R^2=0.59; p<0.001), 3) quantitative relationships between FLIm CH1 LT signal and tensile strength (R^2=0.82; p<0.001), and 4) automated SVM classification of

collagen crosslinking in self-assembled neocartilage using fluorescence-based parameters (discriminant ability of 98.4%).

Biochemical properties of self-assembled articular cartilage were enhanced through matrix stabilization with exogenous LOXL2 and LINK proteins. Increases in proteoglycan content were seen with the addition of LOXL2 and LINK proteins in quantitative assays (1.5- and 1.4-fold, respectively) and qualitatively with increased safranin O staining. While the total collagen content was not significantly altered, matrix stabilization with LOXL2 and LINK proteins resulted in a more aligned collagen fiber orientation as observed in increased collagen birefringence in histological sections. In addition to increased structural alignment, treatment with LOXL2 and LINK increased total crosslinking density in neocartilage by 4.6-fold as compared to control. Because collagen architecture and strength are critical to cartilage function and durability, the exogenous addition of matrix stabilizing proteins like LOXL2 and LINK may be warranted to ensure the long-term success of repair cartilage.

During loading, the collagen network helps resist lateral expansion of the cartilage and creates a mesh-like structure that traps the large, hydrophilic proteoglycan aggregates and allows for osmotic pressure build-up and tissue load-bearing capabilities (Park, *et al.*, 2003). This interplay is dependent on the intrinsic stiffness and strength of each of the matrix components. For cartilage, they depend upon the tensile properties of collagen fibrils and the compressive stiffness of proteoglycan aggregates, as well as the strength of the interfacial bonds among these components. The combination of increased collagen fiber alignment and collagen crosslinking density directly translated into increases in tensile Young's modulus (3.8-fold over control) and ultimate tensile strength (8.3-fold over control). LINK protein has been shown to bind to the bone morphogenetic protein receptor-II (BMP-RII) on chondrocytes, initiating an increased expression of the chondrocyte-specific transcription factor SOX 9 and collagen type-II (Wang, *et al.*, 2013). Through such binding activities, LINK protein may be involved in regulating the content, formation, and the morphology of collagen fibrils. The synergistic increase in collagen crosslinking density with the combination of +LOX+LINK treatment (4.6-fold over control) as compared to +LOX treatment alone (2.4-fold over control) may be partially attributed to the ability of LINK protein to directly regulate cellular biochemical processes in addition to LOX having a known effect on collagen crosslinking. LINK protein has been shown to directly bind fibrillar collagen and increase collagen fiber diameter (Chandrasekhar, *et al.*, 1984) and to bind epidermal growth factor receptors (Spicer, *et al.*, 2003) resulting in increased cartilage mechanical strength (Jia, *et al.*, 2016).

Matrix stabilization improved the compressive properties of the self-assembled neocartilage. Large increases in compressive modulus (3.9-fold over control) were observed with a combination of LOXL2 and LINK protein. The increases in compressive properties with the addition of exogenous proteins may be partially attributed to the role that aggrecan aggregate size plays in determining cartilage mechanical strength. While LINK protein was not found to increase the total GAG content, it has been shown to increase aggrecan aggregate size by providing an almost irreversible tertiary bond between aggrecan and the core protein hyaluronan (Kiani, *et al.*, 2002). Increases in aggregate size have been shown to increase the average strength of the proteoglycan network and ultimately, the tissue itself (Zhu, *et al.*,

1991). In this way, the stabilization of aggregates by LINK protein may play a significant role in maintaining the organization and attachment of the collagen fiber-reinforced proteoglycan matrix and its intrinsic mechanical properties.

Neocartilage constructs with +LOX and +LINK treatments had tensile properties on par with those of native, juvenile femoral cartilage and the compressive relaxation modulus reached 86% of native values (300 kPa compared to 350 kPa for the native tissue) (Paschos, *et al.*, 2017). The lower proteoglycan content at 4 weeks in culture (~7% in neocartilage as compared to ~14% in native tissue) (Paschos, *et al.*, 2017) may partially account for lower compressive stiffness. Self-assembled neocartilage has been shown to increase in proteoglycan content and compressive properties over longer *in vitro* (Ofek, *et al.*, 2008) and *in vivo* (Responte, *et al.*, 2012) culture periods suggesting the possibility that full biomechanical functionality is achievable.

The non-destructive FLIm techniques detected changes in collagen crosslinking density, proteoglycan content, and changes in the tensile and compressive properties of tissue engineered cartilage that occur with matrix stabilization. The strong linear correlations between destructive and non-destructive tests (R^2=0.82 and R^2=0.59 for FLIm versus tensile and compressive properties, respectively) support the hypothesis that non-destructive assessments could be used to infer the differences in the mechanical properties of self-assembled cartilage. We specified that spectral bands at 375–410 nm (CH1) and 515–565 nm (CH3) are important for the assessment of the tensile and compressive properties of tissue engineered cartilage, a finding that will be of high interest for the fields of cell biology and regenerative medicine. The lack of depth-dependent variations in the biochemical composition in the neocartilage reduced bias created by comparing FLIm surface measurements (~300 μm) to full thickness biochemical and mechanical properties. In contrast, native cartilage has a large depth-dependent variation in biochemical composition. When we subjected native tissue to enzymatic treatments to deplete matrix content, we found lower than expected differences in fluorescence signal in cartilage imaged perpendicular to the tissue surface as compared to cartilage imaged in cross-section (Zhou, et al., 2018).

Support vector machine learning (SVM) classification was able to identify LOXL2-induced collagen crosslinking in the self-assembled neocartilage using fluorescence-based parameters. Distinct fluorescence LT distributions for control and LOXL2 crosslinked samples allowed the SVM classifier to distinguish between groups with a discriminant ability of 98.4%. Our work provides a promising proof of principle by demonstrating the predictive power of the SVM to detect differences in collagen crosslinking content with just a small set of variables. This classification approach can be extended to include larger data sets, and incorporate other variables, such as proteoglycan content, to generate an automated system to assess cartilage tissue maturation and determine whether release criteria are met prior to clinical use.

A major challenge in the research and translation of tissue engineered products is the cost and time associated with destructive testing methods. The inexpensive, fiber-based interface of the FLIm-based system can be incorporated into a standard biosafety cabinet for sterile

imaging and repeated measurements of samples (Sherlock, et al., 2018). The ability to continuously monitor tissue quality enables quick adjustments to varying rates of tissue development, the scrapping and restarting of poorly developing tissue, and predictive capabilities of final tissue quality.

4.1. Conclusions

Matrix stabilization using a combination of exogenous LOXL2 and LINK proteins produces robust self-assembled cartilage with increased tensile and compressive properties on par with native tissue. Fluorescence LT is capable of detecting the biological and mechanical changes that occur with matrix stabilization. These data, combined with fiber-optic based instrumentation suggest that FLIm-based tools are a potential non-destructive method for quantitatively monitoring the growth and quality of tissue engineered articular cartilage. The use of continuous monitoring strategies could represent a significant element in reducing costs in research, meeting the FDA regulatory requirements for compliant manufacturing in industry, and as a diagnostic tool in the clinic. The methods presented here can be adapted to other tissue engineering and regenerative medicine applications.

Supplementary Material

Refer to Web version on PubMed Central for supplementary material.

Acknowledgements

References

Alfonso-Garcia A, Haudenschild AK, Marcu L. 2018, Label-free assessment of carotid artery biochemical composition using fiber-based fluorescence lifetime imaging, Biomed Opt Express, 9 (9): 4064–4076. [PubMed: 30615748]

Allen KD, Athanasiou KA. 2006, Viscoelastic characterization of the porcine temporomandibular joint disc under unconfined compression, J Biomech, 39 (2): 312–322. [PubMed: 16321633]

Angheloiu GO, Haka AS, Georgakoudi I, et al. 2011, Detection of coronary atherosclerotic plaques with superficial proteoglycans and foam cells using real-time intrinsic fluorescence spectroscopy, Atherosclerosis, 215 (1): 96–102. [PubMed: 21193196]

Bank RA, Beekman B, Verzijl N, et al. 1997, Sensitive fluorimetric quantitation of pyridinium and pentosidine crosslinks in biological samples in a single high-performance liquid chromatographic run, Journal of chromatography B, Biomedical sciences and applications, 703 (1–2): 37–44. [PubMed: 9448060]

Chandrasekhar S, Kleinman HK, Hassell JR, et al. 1984, Regulation of type I collagen fibril assembly by link protein and proteoglycans, Coll Relat Res, 4 (5): 323–337. [PubMed: 6509889]

Chang C- C, Lin C- J. 2011, LIBSVM: a library for support vector machines, ACM transactions on intelligent systems and technology (TIST), 2 (3): 27.

Descalle MA, Jacques SL, Prahl TJ, et al. 1998, Measurements of ligament and cartilage optical properties at 351 nm, 365 nm and in the visible range (440–800 nm), Laser-Tissue Interaction, Tissue Optics, and Laser Welding III, Proceedings of SPIE, 3195: 280–286.

FDA. Guidance for Industry: Potency Tests for Cellular and Gene Therapy Products. In: Services USDoHaH, editor. 2011.

Fite BZ, Decaris M, Sun Y, et al. 2011, Noninvasive multimodal evaluation of bioengineered cartilage constructs combining time-resolved fluorescence and ultrasound imaging, Tissue Eng Part C Methods, 17 (4): 495–504. [PubMed: 21303258]

Gago N, Perez-Lopez V, Sanz-Jaka JP, et al. 2009, Age-dependent depletion of human skin-derived progenitor cells, Stem Cells, 27 (5): 1164–1172. [PubMed: 19418448]

Gorpas D, Fatakdawala H, Bec J, et al. 2015, Fluorescence lifetime imaging and intravascular ultrasound: co-registration study using ex vivo human coronaries, IEEE transactions on medical imaging, 34 (1): 156–166. [PubMed: 25163056]

Gorpas D, Ma D, Bec J, et al. 2016, Real-Time Visualization of Tissue Surface Biochemical Features Derived From Fluorescence Lifetime Measurements, IEEE transactions on medical imaging, 35 (8): 1802–1811. [PubMed: 26890641]

Han EH, Wilensky LM, Schumacher BL, et al. 2010, Tissue engineering by molecular disassembly and reassembly: biomimetic retention of mechanically functional aggrecan in hydrogel, Tissue Eng Part C Methods, 16 (6): 1471–1479. [PubMed: 20486781]

Hardingham TE. 1979, The role of link-protein in the structure of cartilage proteoglycan aggregates, Biochem J, 177 (1): 237–247. [PubMed: 34388]

Haudenschild AK, Sherlock BE, Zhou X, et al. 2018, Nondestructive fluorescence lifetime imaging and time-resolved fluorescence spectroscopy detect cartilage matrix depletion and correlate with mechanical properties, Eur Cell Mater, 36: 30–43. [PubMed: 30051455]

Haus JM, Carrithers JA, Trappe SW, et al. 2007, Collagen, cross-linking, and advanced glycation end products in aging human skeletal muscle, Journal of applied physiology (Bethesda, Md : 1985), 103 (6): 2068–2076.

Hsu C- W, Lin C- J. 2002, A comparison of methods for multiclass support vector machines, IEEE transactions on Neural Networks, 13 (2): 415–425. [PubMed: 18244442]

Hu JC, Athanasiou KA. 2006, A self-assembling process in articular cartilage tissue engineering, Tissue Eng, 12 (4): 969–979. [PubMed: 16674308]

Huey DJ, Hu JC, Athanasiou KA. 2012a, Unlike Bone, Cartilage Regeneration Remains Elusive, Science, 338 (6109): 917–921. [PubMed: 23161992]

Huey DJ, Hu JC, Athanasiou KA. 2012b, Unlike bone, cartilage regeneration remains elusive, Science, 338 (6109): 917–921. [PubMed: 23161992]

Irrechukwu ON, Reiter DA, Lin PC, et al. 2012, Characterization of engineered cartilage constructs using multiexponential T(2) relaxation analysis and support vector regression, Tissue Eng Part C Methods, 18 (6): 433–443. [PubMed: 22166112]

Jia H, Ma X, Tong W, et al. 2016, EGFR signaling is critical for maintaining the superficial layer of articular cartilage and preventing osteoarthritis initiation, Proceedings of the National Academy of Sciences of the United States of America, 113 (50): 14360–14365. [PubMed: 27911782]

Junqueira LCU, Bignolas G, Brentani RR. 1979, Picrosirius staining plus polarization microscopy, a specific method for collagen detection in tissue sections, The Histochemical Journal, 11 (4): 447–455. [PubMed: 91593]

Kiani C, Chen L, Wu YJ, et al. 2002, Structure and function of aggrecan, Cell Research, 12: 19. [PubMed: 11942407]

Kochiadakis GE, Chrysostomakis SI, Kalebubas MD, et al. 2001, The role of laser-induced fluorescence in myocardial tissue characterization: an experimental in vitro study, Chest, 120 (1): 233–239. [PubMed: 11451844]

Kwon H, Haudenschild AK, Brown WE, et al. 2017, Tissue engineering potential of human dermis-isolated adult stem cells from multiple anatomical locations, PLoS One, 12 (8): e0182531. [PubMed: 28767737]

Lin PC, Irrechukwu O, Roque R, et al. 2012, Multivariate analysis of cartilage degradation using the support vector machine algorithm, Magn Reson Med, 67 (6): 1815–1826. [PubMed: 22179972]

Liu J, Sun Y, Qi J, et al. 2012, A novel method for fast and robust estimation of fluorescence decay dynamics using constrained least-squares deconvolution with Laguerre expansion, Phys Med Biol, 57 (4): 843–865. [PubMed: 22290334]

Mak AF, Lai WM, Mow VC. 1987, Biphasic indentation of articular cartilage--I. Theoretical analysis, J Biomech, 20 (7): 703–714. [PubMed: 3654668]

Makris EA, Gomoll AH, Malizos KN, et al. 2015, Repair and tissue engineering techniques for articular cartilage, Nat Rev Rheumatol, 11 (1): 21–34. [PubMed: 25247412]

Makris EA, MacBarb RF, Responte DJ, et al. 2013, A copper sulfate and hydroxylysine treatment regimen for enhancing collagen cross-linking and biomechanical properties in engineered neocartilage, FASEB J, 27 (6): 2421–2430. [PubMed: 23457219]

Manning HB, Nickdel MB, Yamamoto K, et al. 2013, Detection of cartilage matrix degradation by autofluorescence lifetime, Matrix Biol, 32 (1): 32–38. [PubMed: 23266527]

Marcu L, French PMW, Elson DS. 2014, Fluorescence lifetime spectroscopy and imaging : principles and applications in biomedical diagnostics, CRC Press/Taylor & Francis Group, Boca Raton.

Morgan SP, Rose FR, Matcher SJ. 2014, Optical techniques in regenerative medicine, Taylor & Francis, Boca Raton.

Ofek G, Revell CM, Hu JC, et al. 2008, Matrix development in self-assembly of articular cartilage, PLoS One, 3 (7): e2795. [PubMed: 18665220]

Park S, Krishnan R, Nicoll SB, et al. 2003, Cartilage interstitial fluid load support in unconfined compression, J Biomech, 36 (12): 1785–1796. [PubMed: 14614932]

Paschos NK, Lim N, Hu JC, et al. 2017, Functional properties of native and tissue-engineered cartilage toward understanding the pathogenesis of chondral lesions at the knee: A bovine cadaveric study, J Orthop Res, 35 (11): 2452–2464. [PubMed: 28294398]

Plaas AH, Sandy JD, Kimura JH. 1988, Biosynthesis of cartilage proteoglycan and link protein by articular chondrocytes from immature and mature rabbits, J Biol Chem, 263 (16): 7560–7566. [PubMed: 3372500]

Puchtler H, Waldrop FS, Valentine LS. 1973, Polarization microscopic studies of connective tissue stained with picro-sirius red FBA, Beitr Pathol, 150 (2): 174–187. [PubMed: 4129194]

Responte DJ, Arzi B, Natoli RM, et al. 2012, Mechanisms underlying the synergistic enhancement of self-assembled neocartilage treated with chondroitinase-ABC and TGF-beta1, Biomaterials, 33 (11): 3187–3194. [PubMed: 22284584]

Responte DJ, Natoli RM, Athanasiou KA. 2007, Collagens of articular cartilage: structure, function, and importance in tissue engineering, Crit Rev Biomed Eng, 35 (5): 363–411. [PubMed: 19392643]

Schindelin J, Rueden CT, Hiner MC, et al. 2015, The ImageJ ecosystem: An open platform for biomedical image analysis, Molecular reproduction and development, 82 (7–8): 518–529. [PubMed: 26153368]

Setton LA, Mow VC, Muller FJ, et al. 1993, Altered structure-function relationships for articular cartilage in human osteoarthritis and an experimental canine model, Agents Actions Suppl, 39: 27–48. [PubMed: 8456641]

Seyfried NT, McVey GF, Almond A, et al. 2005, Expression and purification of functionally active hyaluronan-binding domains from human cartilage link protein, aggrecan and versican: formation of ternary complexes with defined hyaluronan oligosaccharides, J Biol Chem, 280 (7): 5435–5448. [PubMed: 15590670]

Spicer AP, Joo A, Bowling RA. 2003, A Hyaluronan Binding Link Protein Gene Family Whose Members Are Physically Linked Adjacent to Chrondroitin Sulfate Proteoglycan Core Protein Genes: THE MISSING LINKS, Journal of Biological Chemistry, 278 (23): 21083–21091. [PubMed: 12663660]

Sun MY, Yoo E, Green BJ, et al. 2012, Autofluorescence imaging of living pancreatic islets reveals fibroblast growth factor-21 (FGF21)-induced metabolism, Biophys J, 103 (11): 2379–2388. [PubMed: 23283237]

Sun Y, Park J, Stephens DN, et al. 2009, Development of a dual-modal tissue diagnostic system combining time-resolved fluorescence spectroscopy and ultrasonic backscatter microscopy, The Review of scientific instruments, 80 (6): 065104. [PubMed: 19566223]

Tang LH, Buckwalter JA, Rosenberg LC. 1996, Effect of link protein concentration on articular cartilage proteoglycan aggregation, J Orthop Res, 14 (2): 334–339. [PubMed: 8648515]

Wagnieres GA, Star WM, Wilson BC. 1998, In Vivo Fluorescence Spectroscopy and Imaging for Oncological Applications, Photochemistry and Photobiology, 68 (5): 603–632. [PubMed: 9825692]

Wang HW, Lin YC, Pai TW, et al. 2011, Prediction of B-cell linear epitopes with a combination of support vector machine classification and amino acid propensity identification, J Biomed Biotechnol, 2011: 432830. [PubMed: 21876642]

Wang Z, Weitzmann MN, Sangadala S, et al. 2013, Link protein N-terminal peptide binds to bone morphogenetic protein (BMP) type II receptor and drives matrix protein expression in rabbit intervertebral disc cells, J Biol Chem, 288 (39): 28243–28253. [PubMed: 23940040]

Woessner JF Jr 1961, The determination of hydroxyproline in tissue and protein samples containing small proportions of this imino acid, Arch Biochem Biophys, 93: 440–447. [PubMed: 13786180]

Yankelevich DR, Ma D, Liu J, et al. 2014, Design and evaluation of a device for fast multispectral time-resolved fluorescence spectroscopy and imaging, The Review of scientific instruments, 85 (3): 034303. [PubMed: 24689603]

Yu W, Liu T, Valdez R, et al. 2010, Application of support vector machine modeling for prediction of common diseases: the case of diabetes and pre-diabetes, BMC Medical Informatics and Decision Making, 10: 16–16. [PubMed: 20307319]

Zhang L, Hu J, Athanasiou KA. 2009, The Role of Tissue Engineering in Articular Cartilage Repair and Regeneration, Critical reviews in biomedical engineering, 37 (1–2): 1–57. [PubMed: 20201770]

Zhou X, Haudenschild AK, Sherlock BE, et al. 2018, Detection of glycosaminoglycan loss in articular cartilage by fluorescence lifetime imaging, J Biomed Opt, 23 (x): xxxx In Press.

Zhu W, Lai WM, Mow VC. 1991, The density and strength of proteoglycan-proteoglycan interaction sites in concentrated solutions, J Biomech, 24 (11): 1007–1018. [PubMed: 1761579]
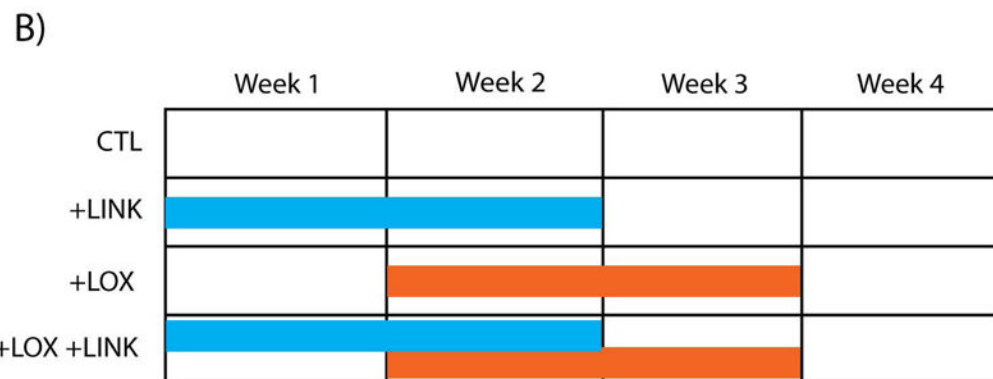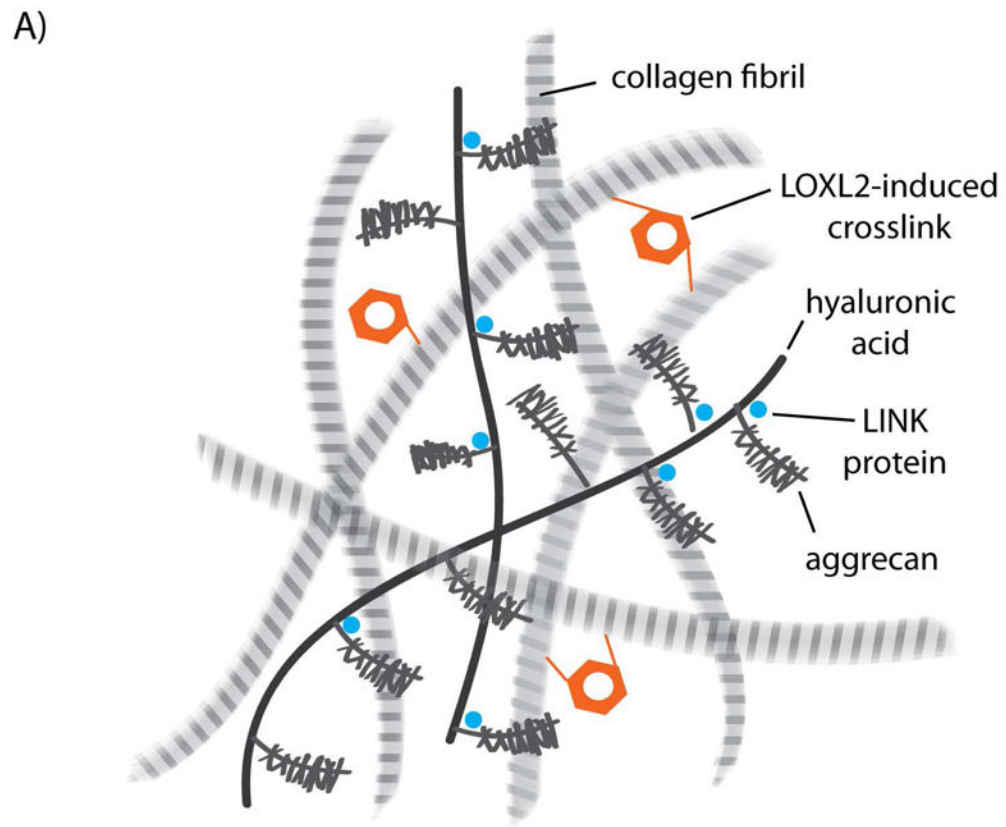
Figure 1.
Schematic overview of the study. A) Articular cartilage ECM. Exogenous addition of LOXL2 protein induces collagen crosslinking while exogenous LINK protein binds aggrecan to the hyaluronic acid backbone of the proteoglycan aggregate. B) Timing and duration of exogenous proteins in each treatment group. +LINK treatment occurred during weeks 0–2, and +LOX treatment occurred during weeks 1–3.
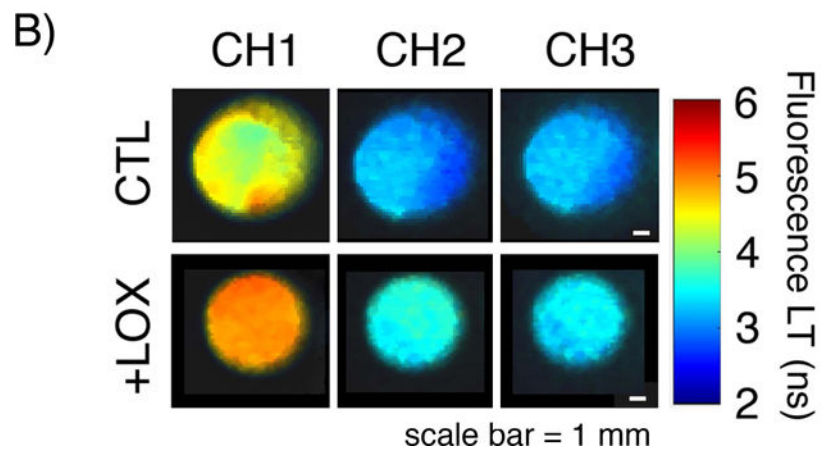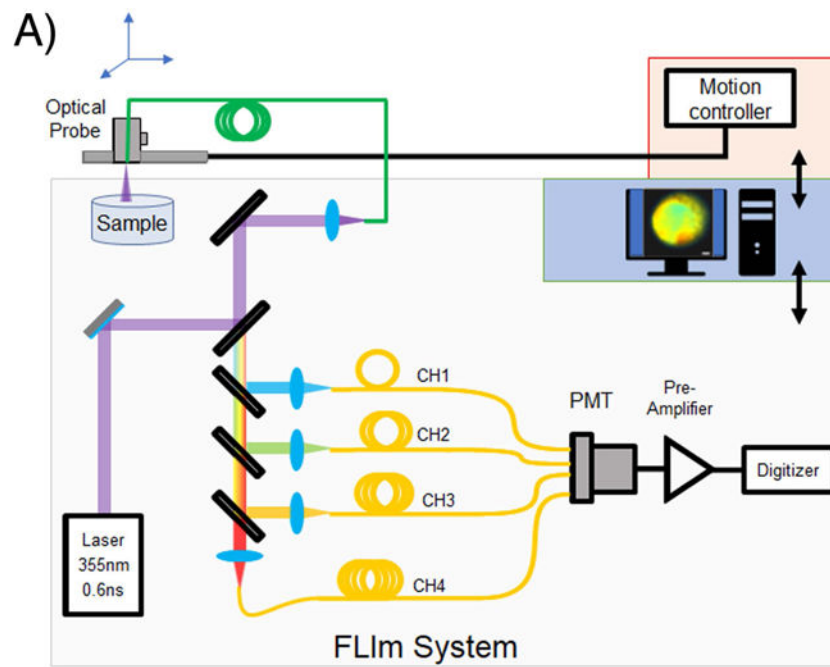
Figure 2.
Optical system for assessing articular cartilage extracellular matrix. A) Schematic of the
FLImTRFS apparatus. A two-axis translation stage was used to scan a fiber optic across the
sample. The fiber guides light from the laser and guides backscattered tissue
autofluorescence to a custom-built wavelength selection module that separates the light into
four spectral channels (CH1 = 375–410 nm, CH2 = 450–485 nm, CH3 = 515–565 nm, CH4
= 595–660 nm). Complete mapping of a 6 mm diameter sample occurs in under 10 minutes
at a resolution of 20 μm/pixel. B) Representative FLIm images of self-assembled constructs

in the CH1, CH2, and CH3 spectral bands show increased LT with +LOX treatment over CTL in all channels.
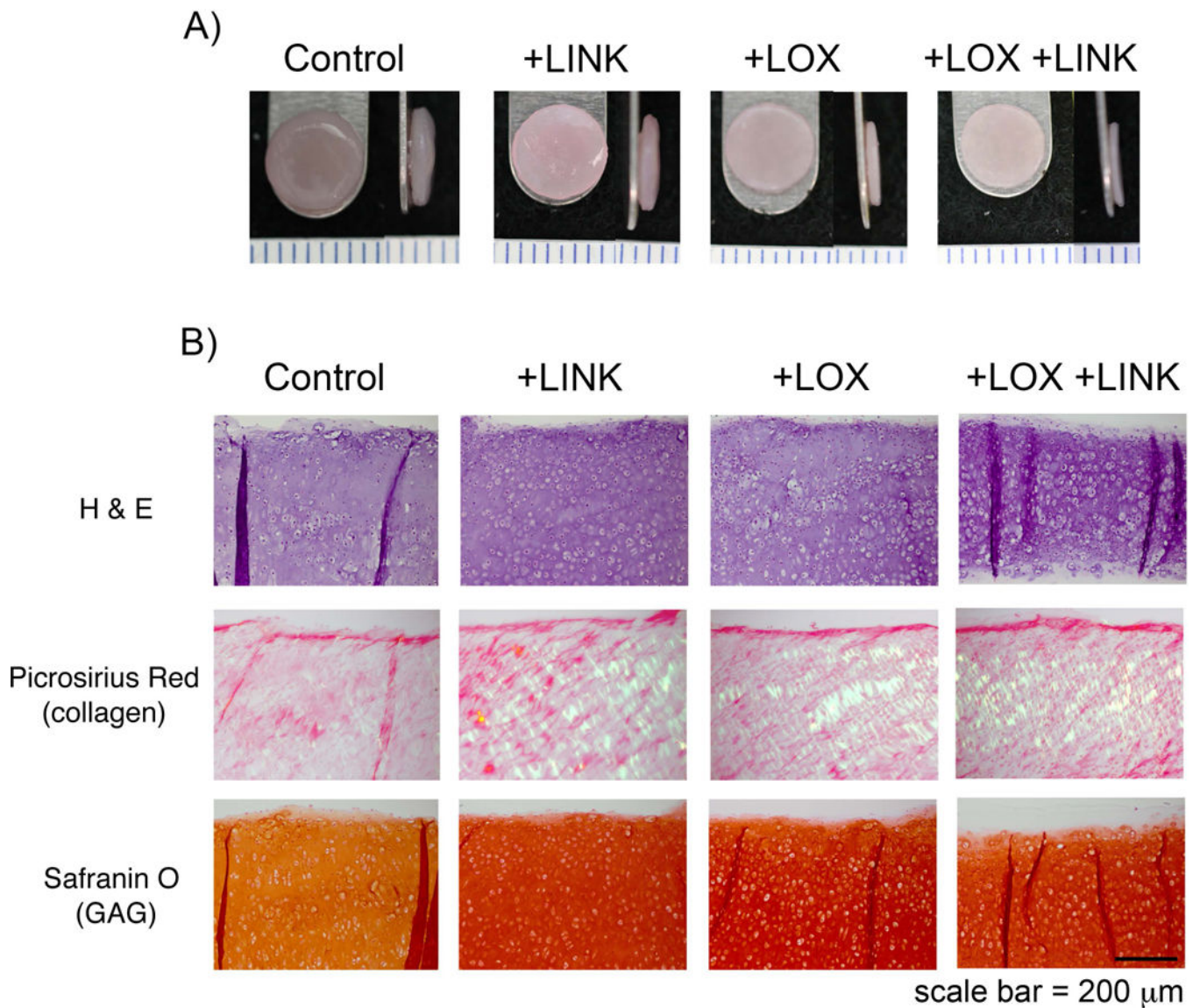
Figure 3.
Enhanced ECM in self-assembled constructs with the addition of exogenous LOXL2 and LINK proteins. A) At 4 weeks, all groups produced uniform, flat constructs. Ruler = 1 mm. B) Histological staining showed increased picrosirius red birefringence and safranin O staining in +LINK, +LOX, and +LOX+LINK groups over control. Scale bar = 200 μm.
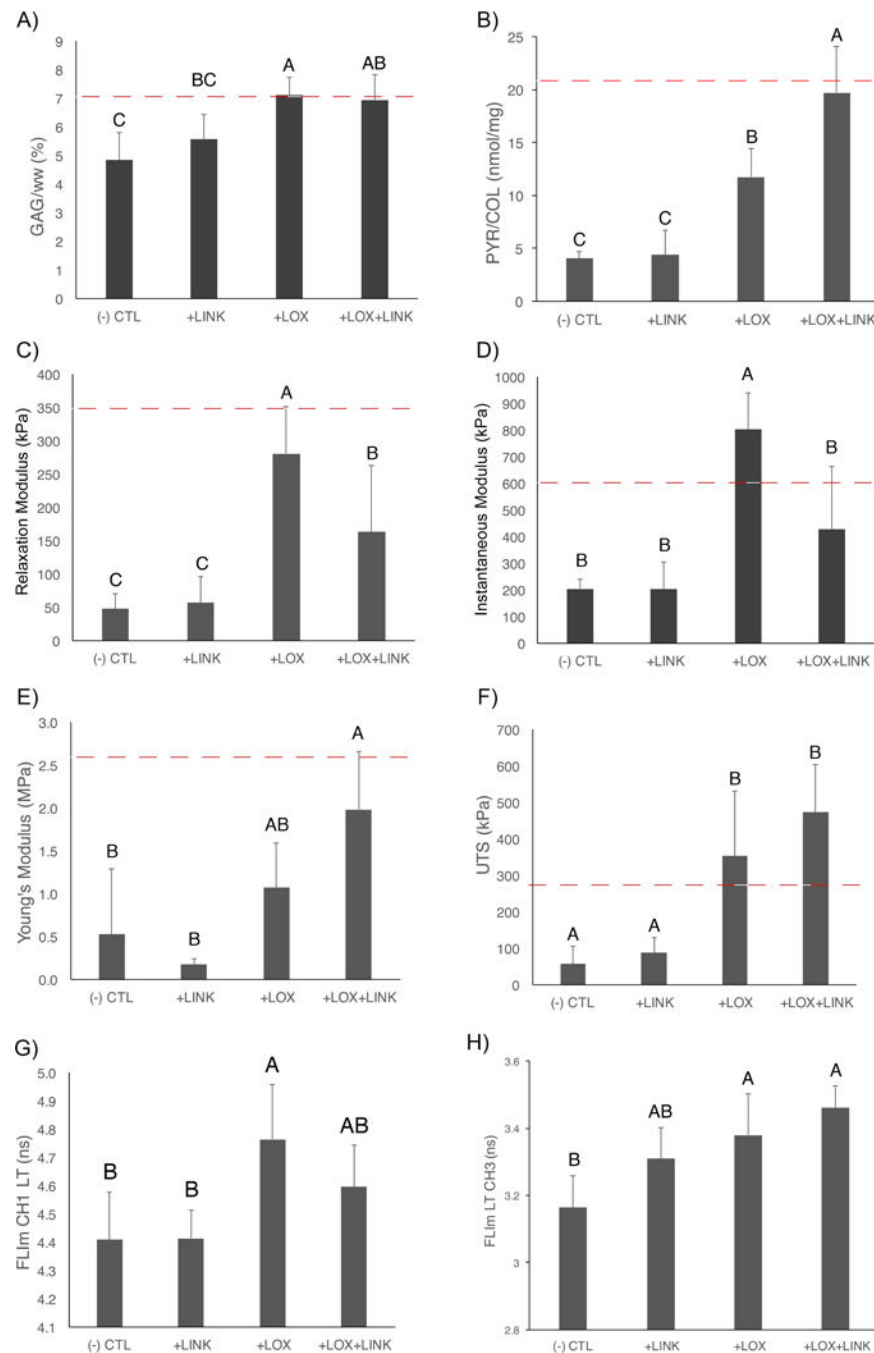
Figure 4.

Matrix stabilization increased biochemical, mechanical, and optical properties of self-assembled neocartilage. A) Proteoglycan content was increased in both +LOX and +LOX +LINK treatments over CTL. B) Collagen crosslinking density was significantly increased with the combined +LOX+LINK treatment over +LOX alone. Both +LOX and +LOX +LINK treatments increased compressive relaxation modulus (C) and ultimate tensile strength (F) over CTL. Instantaneous modulus was increased with +LOX (D) and tensile Young's modulus was increased with +LOX+LINK treatment over CTL. Non-destructive

optical parameter FLIm CH1 LT was significantly increased with +LOX treatment (G) and FLIm CH3 LT was significantly increased with +LOX and +LOX+LINK (H) over CTL. Red dashed lines represent native values (Paschos, et al., 2017).
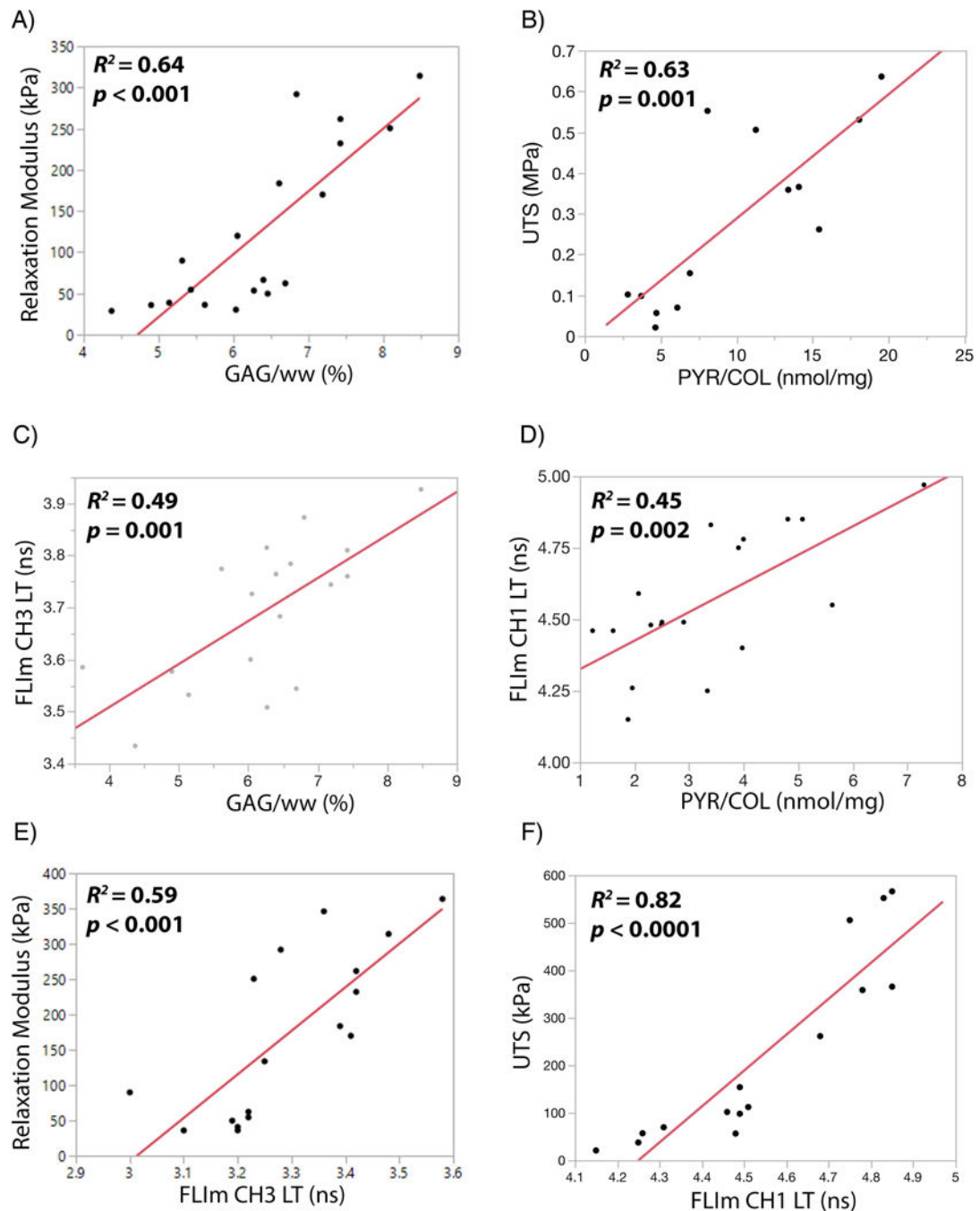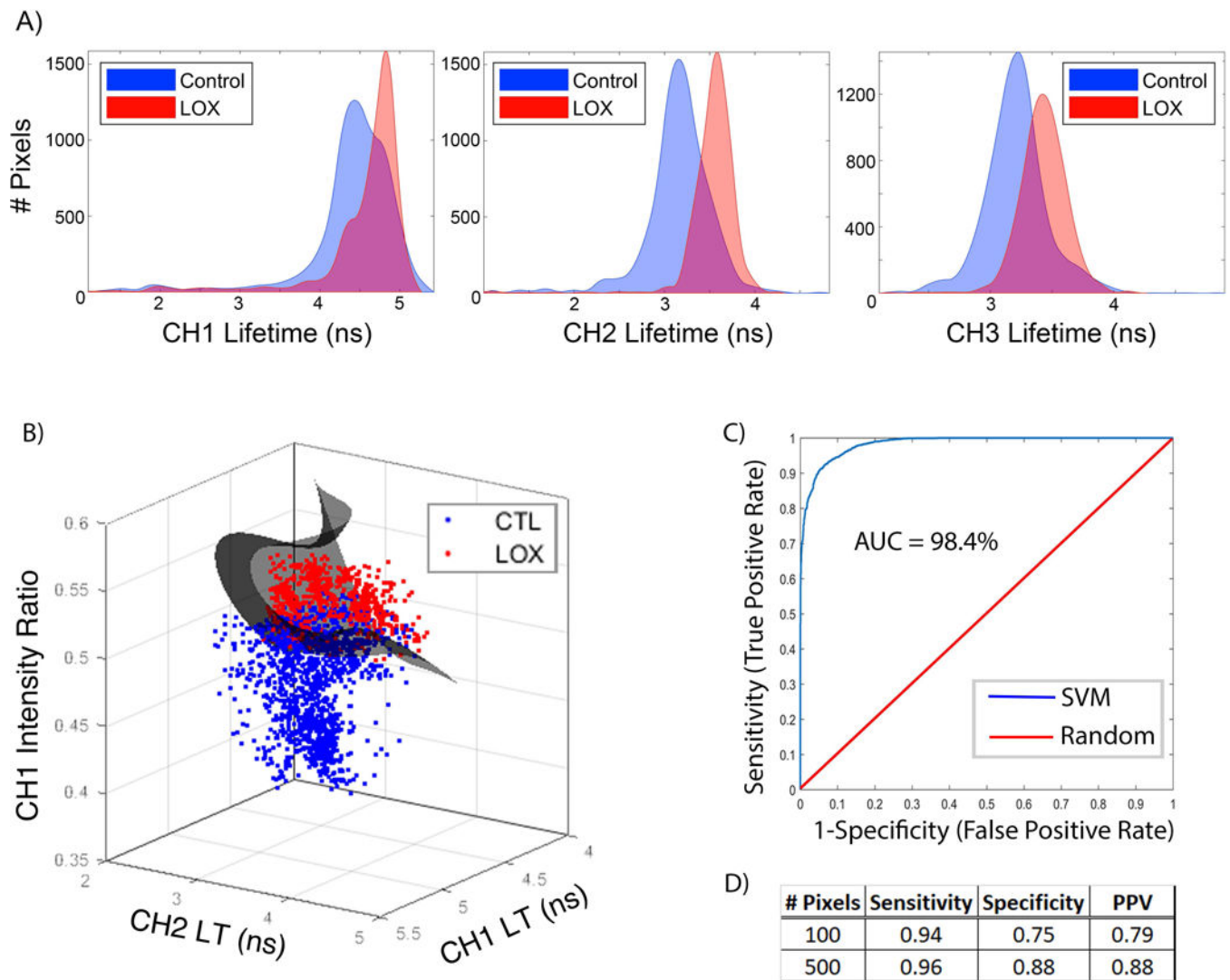
Figure 5.
Destructive and non-destructive tests detect changes in matrix stabilization and mechanical properties. Destructive biochemical assays showed strong correlations between A) compressive relaxation modulus and proteoglycan content (GAG/ww), and B) ultimate tensile strength and collagen crosslinking density (PYR/COL). Non-destructive optical assays showed significant correlations between C) FLIm CH3 LT and GAG/ww, D) FLIm CH1 LT and PYR/COL, E) compressive modulus and FLIm CH3 LT, and F) ultimate tensile strength and FLIm CH1 LT.

Figure 6.
Support vector machine (SVM) learning identifies LOXL2-induced collagen crosslinking in tissue engineered neocartilage. A) Fluorescence LT distributions for control and LOXL2-treated neocartilage in spectral channels CH1, CH2, and CH3 show increased LT with +LOX treatment compared to control. B) Three-dimensional scatter plot of training data for +LOX detection. The SVM classifier hyperplane (grey) acts as a decision boundary for classification. C) Diagnostic ability of the classifier system. A receiver operating characteristic (ROC) curve graphically illustrates the diagnostic ability of the SVM classifier as the discriminant threshold is varied. The discriminant ability of the SVM classifier according to the area under the curve (AUC) is 98.4 %. D) Summary table shoes strong performance values of the support vector machine algorithm for +LOX classification with sensitivity, specificity, and positive predictive value (PPV). Performance increased with increased number of pixels evaluated per sample.